

Probing itinerant carrier dynamics at the diamond surface using single nitrogen vacancy centers

Marjana Mahdia, James Allred, Zhiyang Yuan, Jared Rovny, and Nathalie P. de Leon
Department of Electrical and Computer Engineering, Princeton University, Princeton, New Jersey 08544, USA

(*npdeleon@princeton.edu)

(Dated: 17 October 2022)

Color centers in diamond are widely explored for applications in quantum sensing, computing, and networking. Their optical, spin, and charge properties have been extensively studied, while their interactions with itinerant carriers are relatively unexplored. Here we show that NV centers situated within 10 nm of the diamond surface can be converted to the neutral charge state via hole capture. By measuring the hole capture rate, we extract the capture cross section, which is suppressed by proximity to the diamond surface. The distance dependence is consistent with a carrier diffusion model, indicating that the itinerant carrier lifetime can be long, even at the diamond surface. Measuring dynamics of near-surface NV centers offers a new tool for characterizing the diamond surface and investigating charge transport in diamond devices.

Color centers have been widely studied for their applications in quantum sensing, quantum networks, and quantum information processing¹⁻³. Nitrogen vacancy (NV) centers in diamond in particular are an attractive platform because they exhibit long spin coherence times at room temperature and they allow for off-resonant optical detection and initialization of spin states^{1,4}. Charge state stability and control of NV centers is of particular interest for applications in nanoscale sensing^{5,6}, superresolution microscopy⁷ and long-term data storage⁸. Recent experiments have focused on selectively preparing⁹⁻¹² and reading out¹³⁻¹⁵ particular charge states, as well as studying the impact of charge dynamics on optically detected magnetic resonance^{16,17}. However, the interactions between itinerant carriers and color centers is less well explored, and can strongly impact the color center charge state, ionization dynamics, and spin readout. Such interactions could also be harnessed for new functionality such as electrically detected magnetic resonance,^{18,19} and stabilizing non-equilibrium charge distributions^{20,21}.

Recent work has focused on using itinerant carriers to manipulate color centers in the diamond bulk. For example, it was shown that the optically dark state of a silicon vacancy (SiV) center is SiV²⁻ through charge state readout of NV centers and SiV centers combined with remote optical pumping²². In another example, holes generated by one NV center were captured by another NV center, converting the latter NV center to the neutral charge state²³. Both studies examined NV centers far (>10 μm) from the surface, at which distances surface effects are negligible.

Here we study charge dynamics of shallow NV centers <10 nm from the surface and their interaction with itinerant carriers. Shallow defects are essential for high sensitivity quantum sensing, and understanding the NV charge state and itinerant carrier dynamics near the surface is critical for developing shallow NV centers as a quantum platform. We demonstrate that the charge state of a shallow probe NV center (NV_P) can be controlled by free carriers generated by excitation of another remote shallow source NV center (NV_S) up to $\sim 7 \mu\text{m}$ away (Fig. 1(a, b)). Specifically, the charge state of NV_P converts from negative to neutral as a second 532 nm excitation

laser is scanned over NV_S (Fig. 1(c)). Continuous optical ionization and recombination of NV_S generates a constant flow of holes and electrons in the valence and conduction bands, respectively. These itinerant carriers can diffuse and subsequently be captured by NV_P. The net conversion to the neutral charge state implies that hole capture is much more efficient than electron capture, leading to a net change in the steady-state charge. This phenomenon has been observed in some previous works^{22,23}.

NV centers are individually interrogated using a dual channel, multicolor confocal microscope (see methods). In the experiment, two optically resolvable NV centers are chosen within the scanning field of view, NV_P and NV_S. One optical channel monitors the charge state of NV_P after initialization into NV⁻ with roughly 70% probability using a high power green pulse (94 μW , 5 ms), followed by charge state readout with a low power orange pulse (2 μW , 150 ms). In between these pulses, the second optical channel is used to pump NV_S for a time t_{ON} with a green laser pulse of variable power, cycling its charge state between NV⁻ and NV⁰ (Fig. 2(a)). This cycling generates free carriers that diffuse away and can be subsequently captured by nearby NV centers. The charge state population is measured by obtaining fluorescence with orange excitation since 591 nm is situated in between the zero phonon lines (ZPL) of NV⁻ (637 nm) and NV⁰ (575 nm). A time window shorter than the decay time obtained from the fluorescence trace is defined, over which a histogram of photon counts is drawn. The area under the double Poisson shaped histogram is used to determine the charge state population of NV_P (see Supplementary Material for details).

We interrogate the charge capture kinetics by measuring the charge state of NV_P while varying the excitation power at NV_S. As the excitation power increases, the population of the negative charge state ([NV_P]⁻) decreases (Fig. 2(b)). Moreover, [NV_P]⁻ decays exponentially with the duration of the NV_S excitation pulse, and the decay time constant decreases with increasing excitation power (Fig. 2(c)). Without any excitation at NV_S, there is no change in [NV_P]⁻ over time (Fig. 2(d)). The net decay of [NV_P]⁻ during NV_S illumination indicates that hole capture in the negative charge state dominates

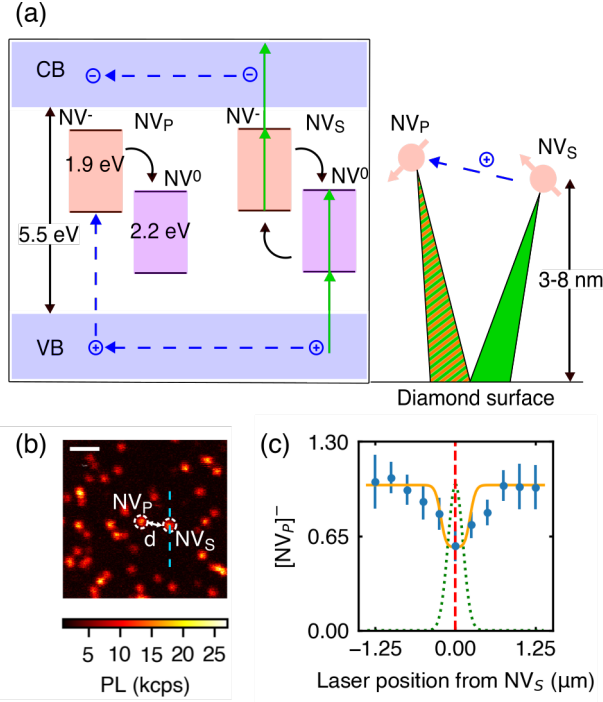


FIG. 1. (a) Energy level diagram showing charge state conversion processes between NV_S and NV_P . Solid vertical arrows indicate photoionization processes, dashed arrows indicate itinerant carrier transport and capture, and curved arrows indicate charge state conversion. (b) Scanning confocal microscope image of two NV centers. The scale bar is $1 \mu\text{m}$. (c) The NV^- charge state population of NV_P as a second laser is scanned along the line cut shown in (b) with the NV_S position indicated with the red dashed line. The orange solid line is a fit considering the dependence of $[NV_P]^-$ on the NV_S excitation laser power. The laser spot size is indicated for reference (green dotted line).

over electron capture in both the negative and neutral charge states.

We model the hole capture rate, γ_h as:

$$\begin{aligned} \gamma_h &= \rho_h c_h + \gamma_d, \\ &= \frac{2\gamma_c e^{-d/L_h}}{4\pi d^2 v_h} \sigma_h v_h + \gamma_d, \\ &= \frac{\sigma_h}{2\pi d^2} \gamma_c e^{-d/L_h} + \gamma_d. \end{aligned} \quad (1)$$

where ρ_h is the hole density, c_h is the capture coefficient, γ_c is the hole generation rate at NV_S , L_h is an effective hole diffusion length that arises from the free carrier lifetime, d is the distance between NV_S and NV_P , σ_h is the hole capture cross-section at NV_P , v_h is the hole velocity, and γ_d is the dark ionization rate, which is constant. The factor of two in the numerator of equation (1) arises from a geometrical factor—we assume that carriers can reflect from the surface, and the NV centers are much closer to the surface than they are to each other. To calculate γ_c (Fig. 2(e)), we first fit the fluorescence of NV_S under 532 nm illumination (after initialization with 591 nm laser) to an exponential fit to extract the total charge

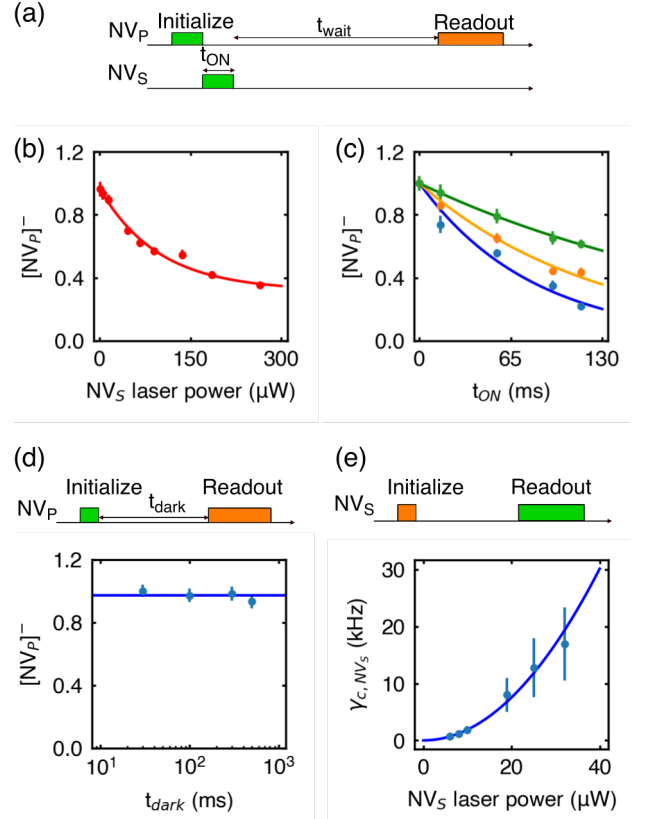


FIG. 2. (a) Pulse sequence used to detect the change of NV_P charge state due to optical excitation of NV_S . A 532 nm laser pulse ($94 \mu\text{W}$, 5ms) initializes NV_P . Another 532 nm pulse (variable power) continuously drives ionization and recombination processes of NV_S for t_{ON} . A 591 nm laser pulse ($2 \mu\text{W}$, 150 ms) is used to readout the charge state of NV_P . A wait time, $t_{wait} = 15$ ms is introduced to avoid background phosphorescence from optical components. (b) Dependence of $[NV_P]^-$ on NV_S excitation laser power ($t_{ON}=15$ ms). The solid line indicates an exponential fit. (c) $[NV_P]^-$ as a function of t_{ON} for different NV_S excitation laser powers (green: $138 \mu\text{W}$, orange: $168 \mu\text{W}$, blue: $216 \mu\text{W}$), $d = 2.6 \mu\text{m}$. Solid lines indicate exponential fits. (d) The stability of the $[NV_P]^-$ in the dark. No change is detected out to 500 ms. (e) Hole generation rate (γ_c) versus green (readout) laser power for NV_S . The fit curve is quadratic, indicating a two photon process.

conversion rate, $\gamma_{total} = \gamma_i + \gamma_r$ of NV_S , where γ_i and γ_r are ionization and recombination rates respectively¹⁶ (see Supplementary Material for details). We measure the NV^- population of several NV centers in our sample at steady state for several powers of 532 nm initialization. All of the measured NV centers show NV^- population in the range of [55%, 70%], which along with γ_{total} is used to calculate γ_r , and subsequently γ_i . In steady state, since the time between subsequent holes is the total time it takes for a hole and an electron to be generated, we have $\gamma_c = (1/\gamma_i + 1/\gamma_r)^{-1}$.

We measured 17 pairs of NV centers in total and observed hole capture in 14 of the pairs (Fig. 3(a)). The hole capture rate varies among pairs of NV centers, and is generally slower for NV pairs with larger spacing d (Fig. 3(b)). This distance dependence could arise from the area scaling of carrier diffu-

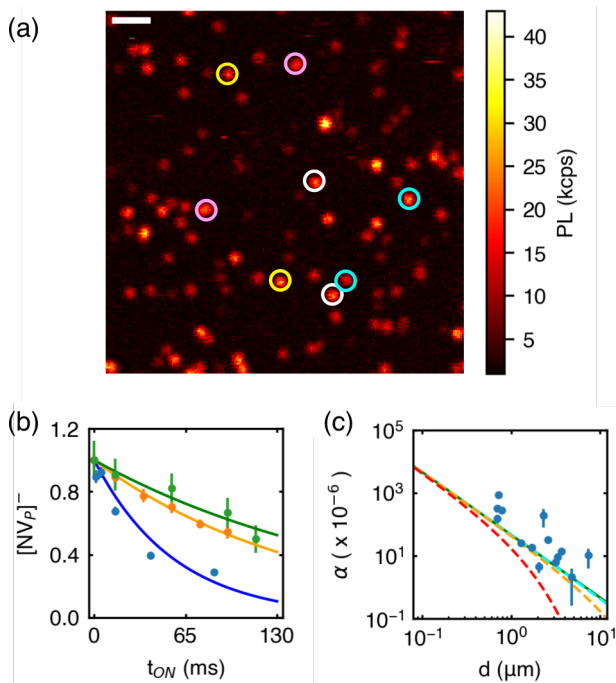


FIG. 3. (a) Confocal scan showing a subset of the NV pairs investigated for calculating σ_h and L_h . Pairs are indicated by different colors. The scale bar is $1 \mu\text{m}$. (b) Time-dependent decay of $[\text{NV}_P]^-$ varies with d (green: $1.71 \mu\text{m}$, orange: $1.29 \mu\text{m}$, blue: $0.70 \mu\text{m}$). NV_S is excited with a $90 \mu\text{W}$ 532 nm laser. Solid lines indicate exponential fits. (c) The ratio of the hole capture rate to the hole generation rate, α , for the 14 different NV pairs under study. The distance dependence is consistent with a diffusion model with an infinite diffusion length (green solid line). For comparison, three dashed lines with finite L_h (cyan: $100 \mu\text{m}$, orange: $10 \mu\text{m}$, red: $1 \mu\text{m}$) are also included.

sion or from a finite carrier lifetime. By rearranging equation (1) we can define a parameter α to investigate if the hole carrier lifetime is an important factor, where

$$\alpha = \frac{\gamma_h - \gamma_d}{\gamma_c} = \frac{\sigma_h e^{-d/L_h}}{2\pi d^2}. \quad (2)$$

We assume $\gamma_d = 0$ because the run time of the experiment ($< 600 \text{ ms}$) is shorter than the dark lifetime of NV_P (Fig. 2(c), see Supplementary Material for details). The calculated α for each NV pair is plotted versus inter-NV distance in Fig. 3(c). The distance dependence is consistent with a $1/d^2$ scaling (see Supplementary Material for details). We therefore conclude that the effective ionization of NV_P due to NV_S is not limited by the diffusion length of holes.

From the fit in Fig. 3(c), we extract the capture cross-section, $\sigma_h = 2.89 \times 10^{-4} \pm 0.54 \times 10^{-4} \mu\text{m}^2$. The large value of σ_h likely arises from the Coulomb attraction between the negatively charged NV center and the hole, resulting in Rydberg-like states²⁴. We note that although the cross section is large, this value is an order of magnitude smaller than previously reported for deep NV centers²³. The surface-related suppression of hole capture could arise from finite hole lifetime due to surface traps or reduction in the effective cross section because

of geometric overlap with the surface. We rule out the former reason based on the distance dependence shown in Fig. 3(c).

We have demonstrated generation and capture of free carriers between two shallow NV centers that are $< 10 \mu\text{m}$ apart from one another. We have shown that the hole capture cross section is smaller than prior measurements of bulk NV centers, but that the observed carrier capture rate is not limited by the carrier lifetime. The hole diffusion length and hole capture cross section can be utilized as sensitive probes of charge transport in diamond devices. The technique demonstrated here can be easily extended to stabilize particular charge states of defects through photo-doping with distant donors, rather than bulk doping, as we have recently demonstrated for SiV^0 centers²¹. A natural next step would be to deploy photodoping to stabilize new color centers such as GeV^0 , SnV^0 and PbV^0 .

METHODS

Diamond samples are prepared using the same process detailed in the previous work²⁵. Diamond substrates from Element Six (E6) are laser cut and scribe polished to a (100) face within a 3 degree specification. They are then reactive ion etched under Ar/Cl_2 and then under O_2 . This etching damage is removed by a 1200°C vacuum anneal. The resulting amorphous carbon layer is removed by refluxing a 1:1:1 mixture of perchloric, nitric, and sulfuric acids for at least two hours (triacid clean). The samples are then implanted with ^{15}N at 3 keV at a dose of $0.5 \times 10^9 \text{ cm}^{-2}$. Following ion implantation, samples are triacid cleaned and then vacuum annealed at 800°C to form nitrogen-vacancy complexes. Following another triacid clean, the samples are then oxygen annealed at 460°C to form a well-ordered oxygen-terminated surface.

To investigate the charge state modification, NV centers are interrogated using multicolor confocal microscope with two excitation pathways. These excitation pathways each pass through two galvanometers (model: Thorlabs GVS012) before being combined into the objective. Photons collected from the sample are counted through two avalanche photodiodes (model: Excelitas SPCM-AQRH-44-FC). This allows for simultaneous optical control and measurement of two distinct NV centers. One excitation path contains only 532 nm laser (laser on NV_S in Fig. 2(a) pulse sequence) from a laser source (model: Coherent Sapphire 532-300 LP), and is used to cycle the charge state of NV_S . The other excitation path (laser on NV_P in Fig. 2(a) pulse sequence) includes light from a continuum source (model: NKT SuperK, repetition rate 78 MHz , pulse width 5 ps), bandpass-filtered at 591 nm , in addition to 532 nm light from another branch of the same green laser source mentioned before. This path is used to interrogate the charge state of NV_P . This setup is similar to the setup used in previous work¹⁶, the primary difference being the path interrogating NV_S .

Laser light sources are coupled into acousto-optic modulators, allowing for pulses with sub 100 ns rise and fall times. A Pulse Blaster (model: SpinCore ESR-PRO500 with a timing resolution of 2 ns) is used to control the acousto-optic modulators and the timing of readout.

The photon count rate depends sensitively on the charge state of the NV center. As a result, a histogram of photon counts per trial reveals two peaks corresponding to the two charge states. Fitting these peaks to a double Poisson distributions then reveals the NV⁻ charge state probability.

SUPPLEMENTARY MATERIAL

See the Supplementary Material for details about determination of NV⁻ population, calculation of carrier generation rate, diagnosis of dark ionization rate, verification of long diffusion length, and hole capture rates for concerned NV centers.

ACKNOWLEDGMENTS

We would like to thank Carlos Meriles and Artur Lozovoi for helpful discussions. This work was primarily supported by the US Department of Energy, Office of Science, Office of Basic Energy Sciences, under Award No. DE-SC0018978. Diamond surface preparation was supported by the NSF under the CAREER program (grant DMR1752047). J.A. acknowledges the NSF Graduate Research Fellowship Program for support. J.R. acknowledges the Princeton Quantum Initiative Postdoctoral Fellowship for support.

AUTHOR DECLARATIONS

Conflict of Interest

The authors have no conflicts to disclose.

Author Contributions

M.M., J.A., J.R., and N.P.d.L. conceptualized the project, designed experiments, analyzed the data, and wrote the manuscript. M.M. and J.A. carried out experiments, Z.Y. and J.R. helped optimize the experimental apparatus and charge state readout. All authors contributed to writing and editing the manuscript.

DATA AVAILABILITY

The data that support the findings of this study are available from the corresponding author upon reasonable request.

REFERENCES

¹L. Childress and R. Hanson, "Diamond nv centers for quantum computing and quantum networks," *MRS bulletin* **38**, 134–138 (2013).

- ²S. Hong, M. S. Grinolds, L. M. Pham, D. Le Sage, L. Luan, R. L. Walsworth, and A. Yacoby, "Nanoscale magnetometry with nv centers in diamond," *MRS bulletin* **38**, 155–161 (2013).
- ³R. Schirhagl, K. Chang, M. Loretz, and C. L. Degen, "Nitrogen-vacancy centers in diamond: nanoscale sensors for physics and biology," *Annu. Rev. Phys. Chem* **65**, 83–105 (2014).
- ⁴N. Bar-Gill, L. M. Pham, A. Jarmola, D. Budker, and R. L. Walsworth, "Solid-state electronic spin coherence time approaching one second." *Nature communications* **4**(1), 1–6 (2013).
- ⁵T. Staudacher, F. Shi, S. Pezzagna, J. Meijer, J. Du, C. A. Meriles, F. Reinhard, and J. Wrachtrup, "Nuclear magnetic resonance spectroscopy on a (5-nanometer) 3 sample volume," *Science* **339**, 561–563 (2013).
- ⁶H. Mamin, M. Kim, M. Sherwood, C. Rettner, K. Ohno, D. Awschalom, and D. Rugar, "Nanoscale nuclear magnetic resonance with a nitrogen-vacancy spin sensor," *Science* **339**, 557–560 (2013).
- ⁷X. Chen, C. Zou, Z. Gong, C. Dong, G. Guo, and F. Sun, "Subdiffraction optical manipulation of the charge state of nitrogen vacancy center in diamond," *Light: Science & Applications* **4**, e230–e230 (2015).
- ⁸S. Dhomkar, J. Henshaw, H. Jayakumar, and C. A. Meriles, "Long-term data storage in diamond," *Science advances* **2**, e1600911 (2016).
- ⁹C. Kurtsiefer, S. Mayer, P. Zarda, and H. Weinfurter, "Stable solid-state source of single photons," *Physical review letters* **85**, 290 (2000).
- ¹⁰L. Rondin, G. Dantelle, A. Slablab, F. Grosshans, F. Treussart, P. Bergonzo, S. Perruchas, T. Gacoin, M. Chaigneau, H.-C. Chang, *et al.*, "Surface-induced charge state conversion of nitrogen-vacancy defects in nanodiamonds," *Physical Review B* **82**, 115449 (2010).
- ¹¹S. Cui and E. L. Hu, "Increased negatively charged nitrogen-vacancy centers in fluorinated diamond," *Applied Physics Letters* **103**, 051603 (2013).
- ¹²C. Schreyvogel, V. Polyakov, R. Wunderlich, J. Meijer, and C. Nebel, "Active charge state control of single nv centres in diamond by in-plane al-schottky junctions," *Scientific reports* **5**, 1–12 (2015).
- ¹³P. Neumann, J. Beck, M. Steiner, F. Rempp, H. Fedder, P. R. Hemmer, J. Wrachtrup, and F. Jelezko, "Single-shot readout of a single nuclear spin," *science* **329**, 542–544 (2010).
- ¹⁴L. Robledo, L. Childress, H. Bernien, B. Hensen, P. F. Alkemade, and R. Hanson, "High-fidelity projective read-out of a solid-state spin quantum register," *Nature* **477**, 574–578 (2011).
- ¹⁵B. J. Shields, Q. P. Unterreithmeier, N. P. de Leon, H. Park, and M. D. Lukin, "Efficient readout of a single spin state in diamond via spin-to-charge conversion," *Physical review letters* **114**, 136402 (2015).
- ¹⁶Z. Yuan, M. Fitzpatrick, L. V. Rodgers, S. Sangtawesin, S. Srinivasan, and N. P. de Leon, "Charge state dynamics and optically detected electron spin resonance contrast of shallow nitrogen-vacancy centers in diamond," *Physical Review Research* **2**, 033263 (2020).
- ¹⁷D. Bluvstein, Z. Zhang, and A. C. B. Jayich, "Identifying and mitigating charge instabilities in shallow diamond nitrogen-vacancy centers," *Phys. Rev. Lett.* **122**, 076101 (2019).
- ¹⁸F. M. Hrubesch, G. Braunbeck, M. Stutzmann, F. Reinhard, and M. S. Brandt, "Efficient electrical spin readout of nv- centers in diamond," *Physical review letters* **118**, 037601 (2017).
- ¹⁹P. Siyushev, M. Nesladek, E. Bourgeois, M. Gulka, J. Hruby, T. Yamamoto, M. Trupke, T. Teraji, J. Isoya, and F. Jelezko, "Photoelectrical imaging and coherent spin-state readout of single nitrogen-vacancy centers in diamond," *Science* **363**, 728–731 (2019).
- ²⁰S. Dhomkar, P. R. Zangara, J. Henshaw, and C. A. Meriles, "On-demand generation of neutral and negatively charged silicon-vacancy centers in diamond," *Physical review letters* **120**, 117401 (2018).
- ²¹Z.-H. Zhang, A. M. Edmonds, N. Palmer, M. L. Markham, and N. P. de Leon, "Neutral silicon vacancy centers in diamond via photoactivated itinerant carriers," *arXiv preprint arXiv:2209.08710* (2022).
- ²²A. Gardill, I. Kemeny, M. C. Cambria, Y. Li, H. T. Dinani, A. Norambuena, J. R. Maze, V. Lordi, and S. Kolkowitz, "Probing charge dynamics in diamond with an individual color center," *Nano Letters* **21**, 6960–6966 (2021).
- ²³A. Lozovoi, H. Jayakumar, D. Daw, G. Vizkelethy, E. Bielejec, M. W. Doherty, J. Flick, and C. A. Meriles, "Optical activation and detection of charge transport between individual colour centres in diamond," *Nature Electronics* **4**, 717–724 (2021).
- ²⁴Z.-H. Zhang, P. Stevenson, G. Thiering, B. C. Rose, D. Huang, A. M. Edmonds, M. L. Markham, S. A. Lyon, A. Gali, and N. P. De Leon, "Optically detected magnetic resonance in neutral silicon vacancy centers in diamond

via bound exciton states,” *Physical review letters* **125**, 237402 (2020).

²⁵S. Sangtawesin, B. L. Dwyer, S. Srinivasan, J. J. Allred, L. V. H. Rodgers, K. De Greve, A. Stacey, N. Dontschuk, K. M. O’Donnell, D. Hu, D. A. Evans, C. Jaye, D. A. Fischer, M. L. Markham, D. J. Twitchen, H. Park,

M. D. Lukin, and N. P. de Leon, “Origins of diamond surface noise probed by correlating single-spin measurements with surface spectroscopy,” *Phys. Rev. X* **9**, 031052 (2019).

Probing itinerant carrier dynamics at the diamond surface using single nitrogen vacancy centers

Marjana Mahdia, James Allred, Zhiyang Yuan, Jared Rovny, Nathalie P. de Leon*

Department of Electrical and Computer Engineering, Princeton University, Princeton, New Jersey 08544, USA

*Email: npdeleon@princeton.edu

October 17, 2022

A. NV^- population determination

To determine the NV^- population of NV_P ($[NV_P]^-$), the pulse sequence in Fig. 2a (main text) is used. After initializing NV_P with a 532 nm laser pulse, another 532 nm laser pulse is used to pump NV_S . During the readout period of NV_P with the orange laser pulse, we see an exponential decay in the fluorescence (Fig. S1 inset). The decay time is determined from an exponential fit of the fluorescence, which defines the length of an integration window. A histogram of photon counts during this window in many experiment iterations is plotted (Fig. S1). The histogram can be fitted with a double Poisson function. The area under the Poisson fit of higher (lower) average photon counts gives us the NV^- (NV^0) population probability of NV_P .

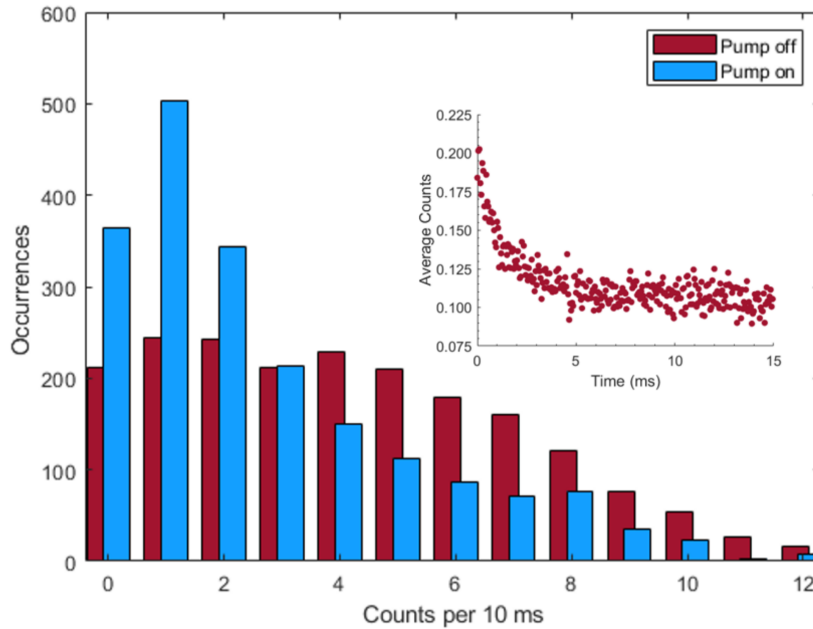


FIG. S1. Determination of $[NV_P]^-$ from double Poisson fit. Blue (red) diagram corresponds to laser on NV_S being ON (OFF).

B. Carrier generation rate calculation

Using the pulse sequence shown in Fig. 2e (main text), the carrier generation rate of NV_S is determined. NV_S is at first initialized into mostly NV^0 charge state with an orange laser, and then a green laser is applied for readout. During the readout, we see an exponential rise in the fluorescence, which can be fitted with an exponential fit (red solid line in Fig. S2). The exponential fit provides us with a rise time, from which we calculate γ_{total} . We have $\gamma_{total} = \gamma_i + \gamma_r$, where γ_i , γ_r , and γ_{total} are the ionization rate, recombination rate, and total rate for a particular excitation wavelength and power, respectively. We calculate γ_r from the equation: $\gamma_r = [NV]^- \gamma_{total} / 100$, where $[NV]^-$ is the steady state NV^- population of NV_S under green excitation. For different powers of green excitation, we measure $[NV]^-$ for several NV centers, which falls in the range of [55%, 70%]. We use this range to calculate γ_r , and subsequently γ_i . We then calculate the hole (or, electron) carrier generation rate, $\gamma_e = \gamma_i \gamma_r / \gamma_{tot}$ for a particular green readout power.

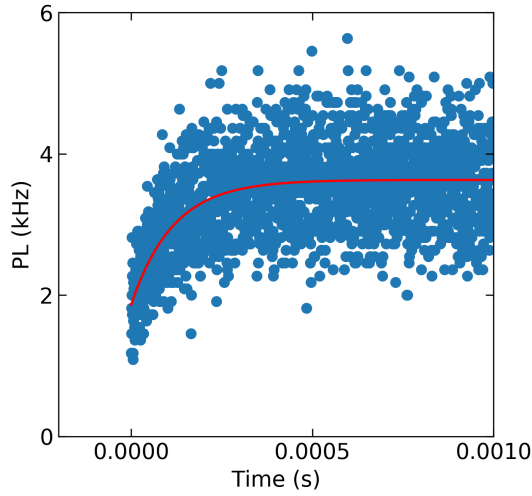


FIG. S2. Calculation of carrier generation rate of NV_S . Red line is an exponentially rising fit of the fluorescence.

C. Dark lifetime of NV_P

The dark lifetime of NV_P could be related to laser leakage, thermal activation, and/or tunneling of the NV center electron to the surrounding trap states (e.g. vacancy complexes, surface traps). To quantitatively understand from our obtained data points whether we can observe the dark lifetime of NV_P in our experiment, we plot β versus d , where $\beta = (\gamma_h/\gamma_c)2\pi d^2$ (Fig. S3). From the plot, we see no gradual rise in the calculated values for longer d . If there was a gradual increase of β with d , the increase would be the result of the dark lifetime of NV_P , as at longer distances, the dark lifetime of NV_P would play the dominant role in its ionization. We also do not observe any decay of β with d , which again supports our conclusion of very long L_h .

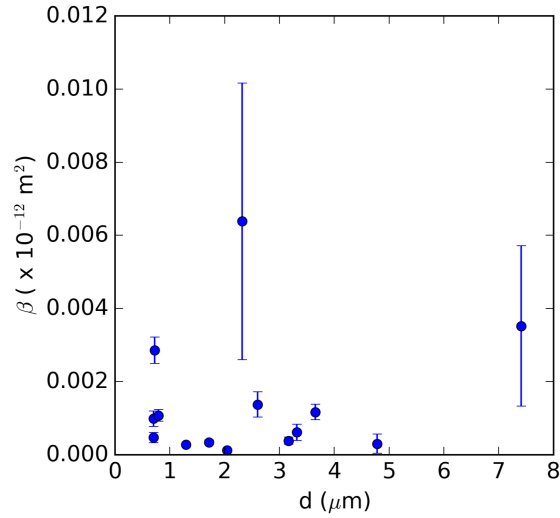


FIG. S3. Diagnosis of dark ionization rate of NV_P . β for 14 different NV pairs are plotted against d to understand the influence of NV_P dark lifetime in our experiment.

D. Verification of long diffusion length from reduced χ^2

To verify long diffusion length from reduced χ^2 , we plot γ_h versus $\gamma_c e^{-d/L_h} / (2\pi d^2)$ after assuming an arbitrary value for L_h (Fig. S4(a)). We then fit the calculated values with a linear fit (red solid line). From the fit we extract reduced χ^2 . We plot the reduced χ^2 for the corresponding L_h (Fig. S4(b)). The reduced χ^2 reduces until it becomes saturated with increasing L_h . The reduced χ^2 saturates for L_h of $\sim 50 \mu\text{m}$, which indicates that the diffusion length is much longer than the inter-NV separations we consider here.

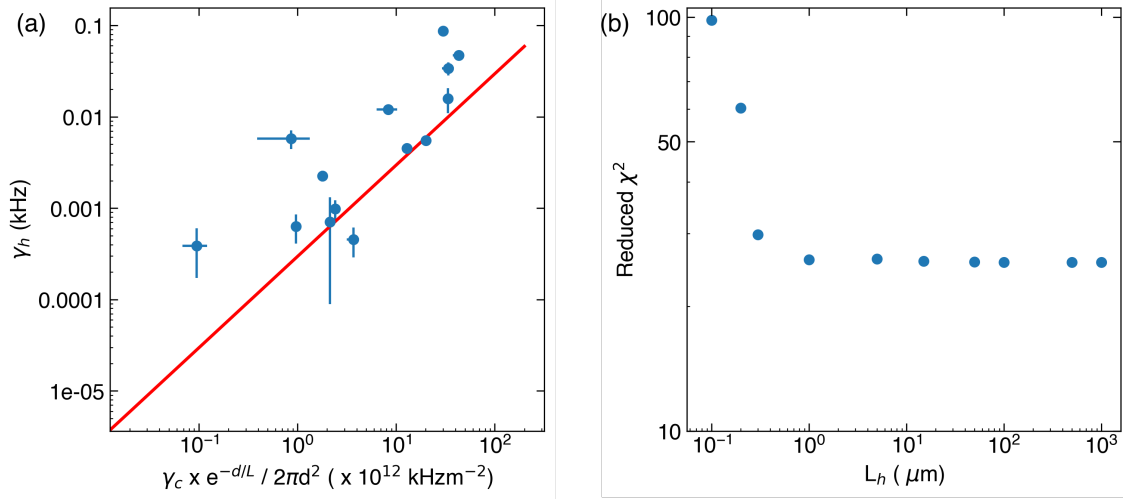


FIG. S4. (a) Plot used to calculate reduced χ^2 for different fit with L_h . In this figure, we assumed L_h to be $50 \mu\text{m}$. Red solid line is a linear fit. (b) Reduced χ^2 calculation from fits assuming different L_h .

E. Tables for the rates in main text figures

I. Fitted values for γ_h in Fig. 2(c) of main text:

NV _S excitation power (μ W)	γ_h (kHz)
138	0.0043 ± 0.0001
168	0.0079 ± 0.0003
216	0.0123 ± 0.0007

II. Fitted values for γ_h in Fig. 3(b) of main text:

d (μ m)	γ_h (kHz)
1.71	0.0049 ± 0.0005
1.29	0.0067 ± 0.0001
0.7	0.0175 ± 0.0020